CARIBBEAN SEA WATER TEMPERATURES OF THE LAST 500 YEARS AS DERIVED FROM SCLEROSPONGES

By

Juan A. Estrella Martínez

A thesis submitted in partial fulfillment of the requirements for the degree of

MASTER OF SCIENCE
IN
MARINE SCIENCES
GEOLOGICAL OCEANOGRAPHY
UNIVERSITY OF PUERTO RICO
MAYAGÜEZ CAMPUS
2013

Approved by:

_____	_____
Clark Sherman, Ph.D. Member, Graduate Committee	Date
_____	_____
Wilson R. Ramírez, Ph.D. Member, Graduate Committee	Date
_____	_____
Amos Winter, Ph.D. President, Graduate Committee	Date
_____	_____
Emmanuel Irizarry-Soto, M.Sc. Graduate School Representative	Date
_____	_____
John M. Kubaryk, Ph.D. Chairperson of the Department of Marine Sciences	Date

Abstract

A high-resolution record of the Caribbean mixed layer temperature at different depths derived from oxygen isotopic ratios obtained from the sclerosponge *Ceratoporella nicholsoni* is presented. Sclerosponges precipitate calcium carbonate skeletons in equilibrium with their surrounding environment and can live at depths down to 200m. The sponges were collected off the coasts of Puerto Rico and St. Croix in northeastern Caribbean Sea. The records obtained extend from the early 1500's to the present and suggest that the northeastern Caribbean was 1-2°C cooler than present during the Little Ice Age. Wavelet analysis of the sclerosponge records indicate that when the total solar irradiance (TSI) reaches a threshold value of 1365.29Wm^{-2} there is a coupling of the eleven-year sunspot cycle with the decadal sclerosponge-derived temperature variability. The findings suggest a local temperature response to TSI of 0.62°C$(W/m^2)^{-1}$ for the 20th century, similar to previously published global values of climate solar sensitivity.

Resumen

Un récord de alta resolución de la temperatura de la capa mixta del Caribe a diferentes profundidades derivadas de proporciones isotópicas de oxígeno obtenidos de la escleroesponja *Ceratoporella nicholsoni* es presentado. Las escleroesponjas precipitan esqueletos de carbonato de calcio en equilibrio con su medio ambiente y pueden vivir a profundidades de hasta 200m. Las esponjas fueron recolectadas en las costas de Puerto Rico y Santa Cruz, en el noreste del Mar Caribe. Los registros obtenidos se extienden desde los años 1500 hasta el presente y sugieren que el noreste del Caribe fue de 1-2°C más frío que el presente durante la Pequeña Edad de Hielo. Análisis wavelet de los registros indican que cuando la irradiancia solar total (IST) alcanza un valor umbral de 1365.29Wm^{-2} existe un acoplamiento del ciclo de once años de manchas solares con la variabilidad decadal de la temperatura derivada de las escleroesponjas. Los resultados sugieren una respuesta de la temperatura local a IST de 0.62°C$(W/m^2)^{-1}$ para el siglo 20, similar a valores mundiales de sensibilidad solar climática anteriormente publicados.

COPYRIGHT

In presenting this dissertation in partial fulfillment of the requirements for a Master in Marine Sciences degree at the University of Puerto Rico, I agree that the library shall make its copies freely available for inspection. I therefore authorize the Library of the University of Puerto Rico at Mayaguez to copy my MS Thesis totally or partially. Each copy must include the title page. I further agree that extensive copying of this dissertation is allowable only for scholarly purposes. It is understood, however, that any copying or publication of this dissertation for commercial purposes, or for financial gain, shall not be allowed without my written permission.

Signed:

Date:

Dedication

To climate change naysayers, for your stubbornness ignited my interest in climate studies.

Acknowlegements

I would like to thank all my committee members, Amos Winter, Clark Sherman, Thomas Miller and Wilson R. Ramírez. Special thanks to Dr. Winter for all his support and insightful guidance in our project for all these years.

I also thanks to the Deep Reef Ecosystems Studies (Deep CRES) project members, Milton Carlo, Michael Nemeth, Hector Ruíz and Ivonne Bejarano, led by Dr. Sherman and Richard Appeldoorn, for their arduous work collecting the specimens used in this research.

Thanks to Augusto Mangini and his student, Sophie Winterhalder for their wonderful work in Heidelberg doing the uranium/thorium analysis. The great results obtained in Dr. Mangini's lab give a lot of credibility to the analysis done on the data obtained.

Thanks a ton to Yelitsa Gonzalez, GASI Lab Instrumentation Specialist (Geology Department, UPRM), for teaching me how to correctly extract the material from the sclerosponges and for patiently analyzing close to two thousand samples in the mass spectrometer because students aren't allowed to work with the machine.

Finally, I want to thank my family for the unconditional love and support the have given me all my life. I love you all.

Table of Contents

List of figures

List of tables

1. Introduction

1.1 General overview

Studying climate variability in the Caribbean region is of importance because it is part of the Western Hemisphere Warm Pool and is teleconnected to the Atlantic and Pacific Oceans, two of Earth's leading sources of climatic variability [*Malmgren et al.*, 1998; *Enfield and Alfaro*, 1999; *Giannini et al.*, 2000; *Chen and Taylor*, 2002] that ultimately determine Caribbean cyclonic activity and Mesoamerican rainfall [*Wang and Enfield*, 2001]. The Caribbean Current serves as a conduit for colder waters entering the Caribbean from the eastern Atlantic through the Portugal and Canary Currents and the North Equatorial Current and waters from the Southern Atlantic coming in the form of the North Brazil Current [*Richardson*, 2005]. Once in the Caribbean, the different currents converge and gain heat before entering the Gulf of Mexico where they continue to eventually form the Gulf Stream and provide enough atmospheric moisture to affect the global troposphere [*Mickler et al.*, 2004; *Minobe et al.*, 2008].

Much of what is known about the way climate operates on decadal to centennial variability comes from proxy archives. However, few paleoceanographic studies had been conducted in the Caribbean region at resolutions high enough to study climate in the annual to decadal time frames. This study presents annually resolved temperature records derived from three sclerosponges living in the mixed layer and extracted from the shelf edge; two off the southwest coast of Puerto Rico and one from the northern coast of St. Croix. Sclerosponges are calcareous sponges that secrete their aragonite skeletons in isotopic equilibrium with their environment, have the advantage of slow growth (100-300 μm/yr) [*Böhm et al.*, 2000] and

provide proxy records of salinity and temperature with a temporal coverage of up to 1000 years of [*Swart et al.,* 1998]. The sclerosponge species used for this research, *Ceratoporella nicholsoni,* is the most common and largest in the Caribbean and possesses a skeleton that is in many ways similar to corals [*Willenz and Hartman,* 1989; *Swart et al.,* 1998].

1.2 Objectives

The main objectives of this research are to determine, by means of isotopic geochemistry, how the average northeastern Caribbean Sea temperature changed at annual, decadal and multidecadal scales in the past 500 years, examine the main frequencies at which the sea temperature operates in order to find the source of the temperature forcing and establish the rate of heat penetration into the water column. By interpreting the chemistry of the sclerosponge skeletons it is possible to examine the temperature changes in the ambient seawater where they lived.

1.3 Literature review

1.3.1 Caribbean climate

The vast majority of tropospheric moisture originates in the tropics, driving the global hydrologic cycle [*Mickler et al.,* 2004]. The Caribbean lies between the two major oceans (Atlantic and Pacific), and is therefore an appropriate location to study the teleconnections between their respective climate forcings. *Enfield and Alfaro* [1999] and *Giannini et al.* [2000] found that Caribbean rainfall is more closely associated with the sea surface temperature anomaly (SSTA) of the tropical Atlantic than it is with tropical eastern Pacific. Despite this, the amount of rainfall over the Caribbean and northern South America appears to depend on how the SSTA of the tropical Atlantic and eastern Pacific combine, with the

strongest response occurring when the tropical Atlantic is in an antisymmetric meridional dipole configuration across the ITCZ and the eastern Pacific is of opposite sign to the tropical North Atlantic [*Enfield and Alfaro,* 1999].

There is a direct link between North Atlantic sea level pressure (SLP) and Caribbean precipitation by changing the patterns of surface flow over the region. Anomalously high SLP in the region of the North Atlantic high causes the trade winds to gain strength which in turn causes cooler sea surface temperatures (SST) and less Caribbean precipitation [*Giannini et al.,* 2000]. Moreover, when low SLP conditions govern the eastern equatorial Pacific, high SLP conditions thrive over the tropical Atlantic [*Giannini et al.*, 2000] which is in agreement with the results of *Enfield and Alfaro* [1999].

The Caribbean region is dominated by dry winters and wet summers, with the rainy season starting in May and ending in November with a mid-summer precipitation break near the months of July and August. The rainy season gets extended in years that begin with warm SST in the tropical North Atlantic as it starts earlier in spring and ends later in fall. The end dates are also delayed when the equatorial Pacific is cool [*Enfield and Alfaro,* 1999].

Giannini et al. [2000] argue that much of the precipitation variability in the Caribbean can be attributed to El Niño-Southern Oscillation (ENSO) or the North Atlantic sub-tropical high. On the other hand, *Chen and Taylor* [2002] found a significant mode that accounts for almost 50% of Caribbean precipitation that is well correlated with Pacific equatorial anomalies if lagged by one or two seasons. Warm winter anomalies in the NINO3 and NINO4 (5°S-5°N, 90°W-150°W and 120°W-170°W, respectively) regions are related to

positive spring rainfall anomalies in the Caribbean basin south of 20°N [*Chen and Taylor*, 2002]. This occurs when the warm phase of ENSO shifts the subtropical jet stream equatorwards drawing convective outflows northward from the Intertropical Convergence Zone (ITCZ) and South American monsoon [*Jury et al.*, 2007]. ENSO also has a significant effect on the annual mean air temperatures over the Caribbean [*Malmgren et al.*, 1998].

A great amount of climate variability in the interannual to interdecadal time scale in the Atlantic sector is linked to the North Atlantic Oscillation (NAO), a natural mode of climate variability that accounts for ~33% of the variance in SLP [*Cullen et al.*, 2001]. Reconstructions since 1911 show that the NAO influence on Caribbean precipitation amounts are synchronous with variations in the NAO during the winter and are not controlled by ENSO [*Malmgren et al.*, 1998]. A negative, nonpersistent, correlation exists between high winter NAO indices and annual precipitation in Puerto Rico [*Malmgren et al.*, 1998; *Jury et al.*, 2007].

The instrumental record of the last 150 years in the North Atlantic shows a SSTA range of 0.4°C with a periodicity ranging from 55-80 years known as the Atlantic Multidecadal Oscillation (AMO) [*Enfield et al.*, 2001; *Gray*, 2004]. The AMO has been linked to precipitation anomalies (both positive and negative) ranging over multiple years in the Northern Hemisphere [*Enfield et al.*, 2001] and appears to modulate ENSO teleconnections [*Gray*, 2004]. Modeled results also show that variations in the North Atlantic SSTA are linked to tropospheric vertical shear in the main hurricane development region which suggests a link between the AMO and Atlantic hurricane formation [*Knight et al.*, 2006]. Changes in the strength of the Atlantic meridional thermohaline circulation have been proposed as a mechanism controlling the AMO [*Latif et al.*, 2004].

1.3.2 Sclerosponges as a climate proxy

Ceratoporellidan sponges appear to grow in a similar way to corals, as the living tissue only inhabits the upper 1mm of the skeleton [*Hickson*, 1911; *Swart et al.*, 1998]. The tissue extends into the skeleton in conical projections that fill each calicle of the skeleton [*Willenz and Hartman*, 1989]. *Willenz and Hartman* [1989] describe the inhalant and exhalant canals of *Ceratoporella nicholsoni* as being characterized by the presence of valvules that are made by transverse lemellipodial processes of the endopinacoytes that line them. These valvules probably regulate the water flow though the sponge. *C. nicholsoni* also produces rough intercellular fibrils characterized by periodically spaced thickenings [*Willenz and Hartman*, 1989]. An alga from the *Ostreobium sp.* grows on the sponge but it does not interfere with its development [*Willenz and Hartman*, 1989; *Swart et al.*, 1998]. The precipitation of the aragonite skeleton occurs essentially at two sites: primary calcification occurs at the base of the pseudocalices and secondary calcification occurs at the apex of the walls separating the pseudocalices [*Swart et al.*, 1998]. Synthesis and export activities are indicated by the abundance of vesicles which appear to be discharged toward the skeleton and are presumed to build the skeletal organic matrix [*Willenz and Hartman*, 1989].

Arguably, sclerosponges are more advantageous climate proxies than corals. First, the environmental signals obtained from corals may be biased by physiological variables like growth rate, calcification and photosynthesis (shown by *Reynaud-Vaganay et al.* [2001] to be a significant factor). Second, the rapid growth rate of ~0.2–5.0cm/yr means that in order to obtain a long time series one would need to analyze several meters of coral core. Third, density variations within the coral skeleton interfere with high resolution analysis. And finally, zooxanthelate corals are generally restricted to the euphotic layer limiting their

usefulness when investigating environmental changes versus depths throughout the mixed layer. Furthermore, *Rosenheim et al.* [2004] found that sclerosponges are, in fact, better temperature recorders than zooxanthellate corals based on the Sr/Ca sensitivity of each organism, sclerosponges showing nearly twice the sensitivity compared to corals.

The slow growth rate of sclerosponges (100–300μm/yr) [*Swart et al.*, 1998, 2002; *Böhm et al.*, 2000; *Lazareth et al.*, 2000; *Haase-Schramm et al.*, 2003; *Rosenheim et al.*, 2005]; means that even small specimen can be centuries old. The massive sclerosponge skeleton is composed of continuous and dense tufts of aragonite that allow high resolution analysis [*Lazareth et al.*, 2000]. Sclerosponges lack photosynthetic symbionts. This allows them to live at great depths well below the euphotic zone [*Swart et al.*, 1998; *Böhm et al.*, 2000; *Lazareth et al.*, 2000]. Dissolved atmospheric CO_2 represents the source material for carbon atoms in the sclerosponge skeletal carbonate [*Hughes and Thayer*, 2001]. It has been shown in numerous investigations that the oxygen isotopic composition of the sponge's carbonate is related to ambient seawater temperature and salinity [*Swart et al.*, 1998, 2002; *Böhm et al.*, 2000; *Hughes and Thayer*, 2001; *Haase-Schramm et al.*, 2003]. On the other hand, the carbon isotopic composition of the sponge's skeleton can help determine the rate timing of the input of anthropogenic CO_2 into the ocean [*Swart et al.*, 1998, 2002; *Böhm et al.*, 2000; *Hughes and Thayer*, 2001]. Carbon isotope records from corals show a similar pattern but changes may be masked by vital effects [*Swart et al.*, 1998; *Reynaud-Vaganay et al.*, 2001].

Numerous investigations show that the burning of fossil fuels and subsequent increase of CO_2 in the atmosphere causes a decrease in the ratios of stable carbon isotopes in the oceans [*Swart et al.*, 1998, 2002; *Böhm et al.*, 2000; *Lazareth et al.*, 2000]. This is generally

known as the Suess Effect which caused an average decrease in $\delta^{13}C$ over the last 200 years of 0.5 ‰ (Section 2.2) [*Lazareth et al.,* 2000; *Swart et al.,* 2002]. Nearly all sclerosponges show similar rates of $\delta^{13}C$ depletion over the last 200 years and thus the curve tie points can be used to date the sponges. Two points can be taken from the $\delta^{13}C$ profile to construct a preliminary age model: the point where the decrease of $\delta^{13}C$ is first evidenced, which occurred in the mid-17th century for sponges collected in the mixed layer [*Lazareth et al.,* 2000; *Böhm et al.,* 2002; *Swart et al.,* 2002], and the year of collection of the specimen.

Unlike corals, most sclerosponges do not present annual banding in their skleletons so dating them must rely on different methods. In order to obtain an age model *Swart et al.* [2002] used changes in the concentration of Pb (shown by *Lazareth et al.* [2000] to be analogous to results acquired from ice cores and corals), changes in $\delta^{13}C$ and U/Th dates and obtained a mean growth rate of 220μm/yr. However, growth may not always be linear [*Swart et al.,* 2002; *Böhm et al.,* 2000].

Sclerosponges incorporate an order of magnitude more lead than corals [*Rosenheim et al.,* 2005] primarily because they rely uniquely on filter feeding to obtain their nutrition [*Willenz and Hartman,* 1989] while corals obtain their nutrition also from their algal symbionts. The increase of atmospheric Pb concentrations began mid-18th century with a threefold increase in concentration at the height of production which occurred in the early 20th century with the extended use of leaded gasoline [*Lazareth et al.,* 2000; *Rosenheim et al.,* 2005]. Pb made its way to the ocean by wet deposition of aerosols and river transport of particulate matter. A subsequent drop in lead concentration occurs in the 1970s when lead was banned in gasoline in the USA. Lead production recorded in sclerosponges can thus be a useful dating tool [*Lazareth et al.,* 2000].

2. Methodology

2.1 Specimen collection and preparation

The sclerosponges for this study were retrieved south of La Parguera, Puerto Rico from water depths of 36 m and 47 m, and Cane Bay, St. Croix from a depth of 69 m (Figure 1). The sponges were collected by SCUBA divers using rebreather equipment from the Deep Coral Reef Ecosystems Studies (Deep CRES) project located at La Parguera [*Sherman et al.*, 2009].

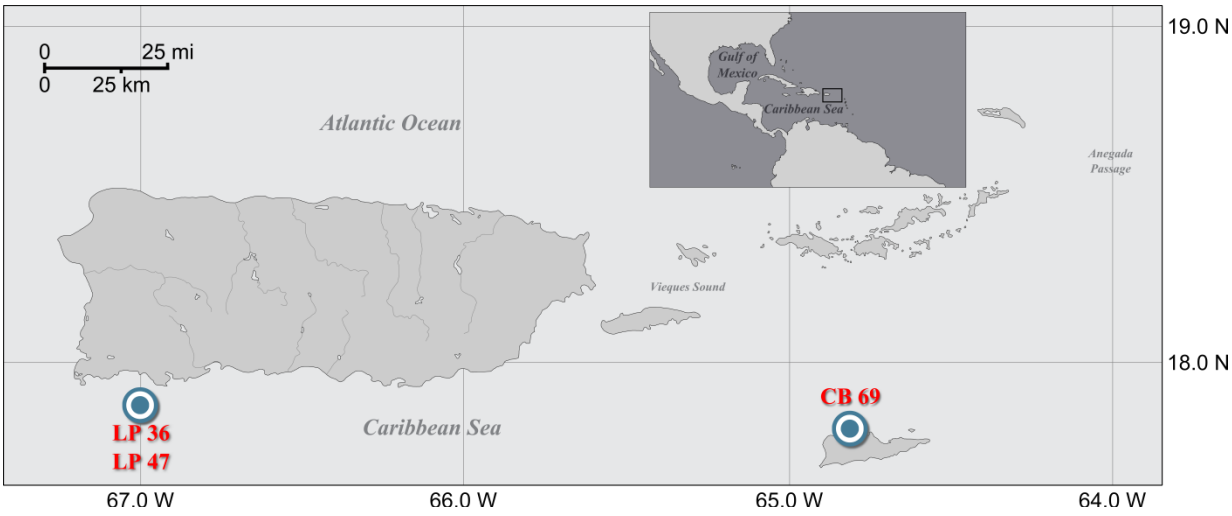

Figure 1 Location of the collection sites of the specimens used in this research.

On land the sclerosponges were cut into slabs (0.5 to 1.0cm thick) and polished (Figure 2). Powder samples from the carbonate sponges were extracted using a New Wave™ micromill with a SS White® carbide bur. The milling channel, along a growth axis, was 2.0mm wide and 0.6mm deep and the sampling resolution was 100µm. The milling drill rotation was held at 5240rpm to avoid any possible aragonite-to-calcite transformations [*Gill et al.*, 1995; *Foster et al.*, 2008].

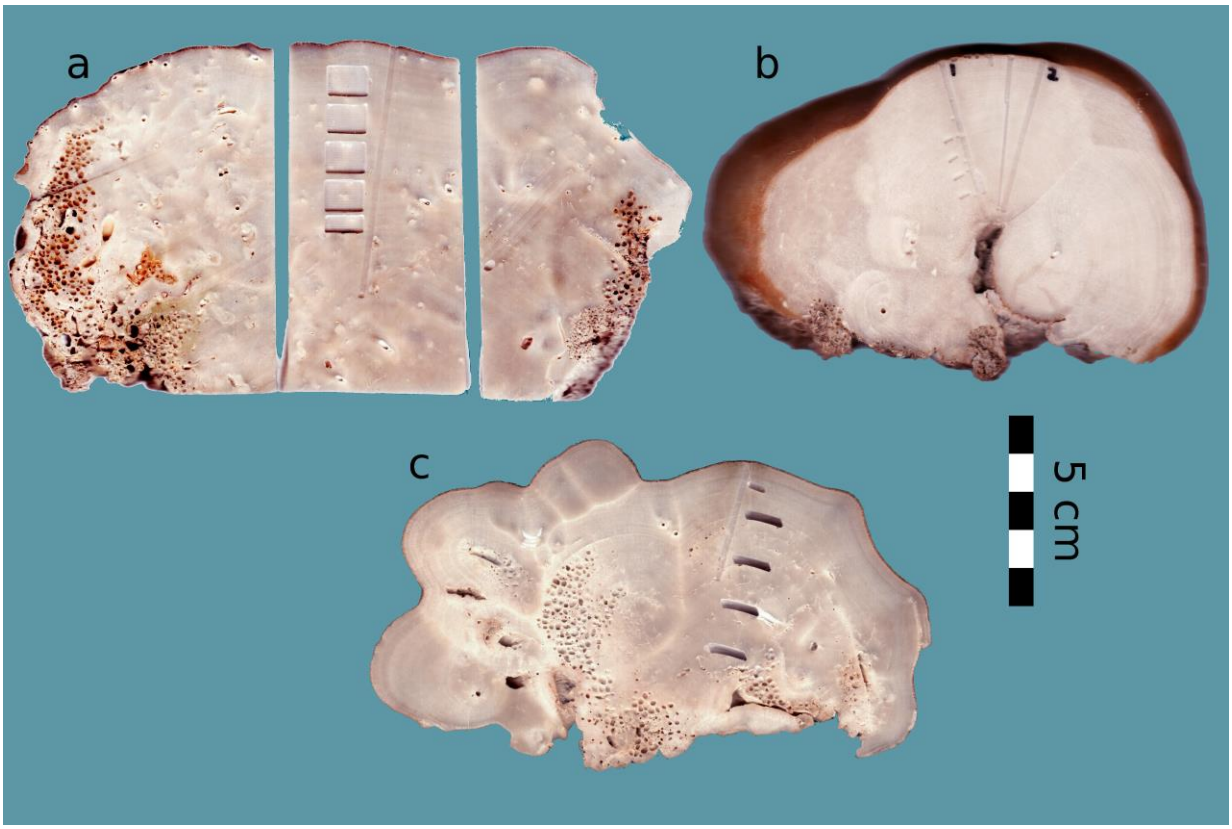

Figure 2 Slabs of the sclerosponges used for this research. The slabs from the specimens collected at 47m (a) and 69m (c) show the pits where the collection of material was done for U/Th dating and their milling canals. The slab of the 3m specimen (b) shows the canals that were milled into it

2.2 Calcium carbonate analysis

Sclerosponges incorporate various chemical parameters which can provide information on the environmental conditions where they grew. The most common of these are the isotopic ratio of ^{18}O to ^{16}O ($\delta^{18}O$) and the isotopic ratio of ^{13}C to ^{12}C ($\delta^{13}C$) that are incorporated into their calcium carbonate. These ratios are then compared to the ratio of a reference material:

$$\delta^{18}O = \left(\frac{\left(\frac{^{18}O}{^{16}O}\right)_{Spl}}{\left(\frac{^{18}O}{^{16}O}\right)_{Std}} - 1 \right) \times 1000 \quad (1)$$

$$\delta^{13}C = \left(\frac{\left(\frac{^{13}C}{^{12}C}\right)_{Spl}}{\left(\frac{^{13}C}{^{12}C}\right)_{Std}} - 1 \right) \times 1000 \quad (2)$$

The units for equations 1 and 2 are given in 'per mil' (‰). The $\delta^{18}O$ and $\delta^{13}C$ values were obtained by analyzing the $CaCO_3$ powder acquired from the sponge's skeleton by mass spectrometry.

The carbonate powder was the reacted with 100% phosphoric acid to obtain CO_2 gas:

$$2H_3PO_{4(aq)} + 3CaCO_{3(s)} \rightleftharpoons Ca_3(PO_4)_{2(aq)} + 3H_2O_{(l)} + 3CO_{2(g)} \quad (3)$$

The CO_2 gas was injected into a Micromass™ IsoPrime magnetic sector isotope ratio mass spectrometer housed in the Geology Department, University of Puerto Rico at Mayagüez to obtain the carbon and oxygen isotopic ratios. Inside the mass spectrometer the gas molecules are converted to ions in a vacuum, and then accelerated by a high voltage through a magnetic field, which causes the ions to curve. The radius of the curve depends on the mass of the ion. Detectors (Faraday cups) are positioned to measure the beam size corresponding to the different masses. This allows the relative abundances, or stable isotope ratios to be measured. The ratios are then compared with a virtual standard, Vienna PeeDee Belenmite (VPDB). Every 6th sample introduced in the mass-spectrometer was the in-house standard, NBS-19, with a $\delta^{18}O$ value of -2.2‰ and a $\delta^{13}C$ value of 1.95‰ when compared to VPDB [*Stichler*, 1995; *Coplen*, 1996]. Using the NBS standard improved precision based on machine drift and also helped keep track of the equipment accuracy.

The objective of skeletal analysis is to obtain a time series of the isotopic ratios recorded perpendicular to the growth layers. *Böhm et al.* [2000] showed that each layer deposited at a given time in sclerosponges contains the same isotopic ratios as ambient seawater. The sensitivity of this mechanism is sufficient that it allows for high resolution reconstructions to be obtained.

2.3 Chronology

Marine and terrestrial carbonates younger than 600kyr can be precisely dated by U-series disequilibrium methods. These methods are based on the natural chain of radioactive decay of radionucleoides. The three decay chains start with an actinide nuclide (^{238}U, ^{235}U and ^{232}Th) that has a long half-live ($T_{1/2}$). All actinide nuclides used have a $T_{1/2}$ greater than 7×10^8yr [*Scholz and Hoffmann*, 2008]. A system will achieve radioactive equilibrium between parent and daughter nuclides in a few million years if it's undisturbed. If this process is interrupted then there is disequilibrium between the activity of the parent and the daughter isotopes. It is the return to equilibrium that can be measured and give us the dating of the moment of equilibrium disruption. Disequilibrium in the ^{238}U decay chain occurs as a result of elemental fractionation of Th from U or isotope fractionation between ^{234}U and ^{238}U [*Scholz and Hoffmann*, 2008].

The different geochemical behavior of U and Th is responsible for the elemental fractionation. U exists on Earth mainly as U^{6+} and it's soluble as uranyl ion and uranyl carbonate [*Scholz and Hoffmann*, 2008]. Uranium in seawater exists as $UO_2CO_3^0$ (20%) and $UO_2(CO_3)_2^{2-}$ (80%) [*Rosenheim et al.*, 2005]. On the other hand, Th is insoluble in natural waters and it is transported in minerals or absorbed onto particles [*Scholz and Hoffmann*,

2008]. This means that there is dissolved U in natural water but no Th. U is then incorporated as a lattice impurity [*Rosenheim et al.*, 2005], creating a disequilibrium between U and Th.

U-series dating requires a measurement of the relevant U and Th isotope abundances to obtain the isotope activity ratios to calculate an age. This calculation can be done by solving the following equations:

$$\left(\frac{^{234}U}{^{238}U}\right)(t) = \left(\left(\frac{^{234}U}{^{238}U}\right)_0 - 1\right)e^{-\lambda_{234}t} + 1 \tag{4}$$

$$\left(\frac{^{230}Th}{^{238}U}\right)(t) = \left(1 - e^{-\lambda_{230}t}\right) + \left(\left(\frac{^{234}U}{^{238}U}\right)(t) - 1\right)\frac{\lambda_{230}}{\lambda_{230} - \lambda_{234}}\left(1 - e^{-(\lambda_{230} - \lambda_{234})t}\right) \tag{5}$$

where $(^{234}U/^{238}U)_0$ is the initial $(^{234}U/^{238}U)$ activity ratio and λ_n is the decay constant $(\ln(2)/T_{1/2})$ for ^{230}Th and ^{234}U [*Scholz and Hoffmann*, 2008]. The measurement of the isotope abundance is usually done by mass spectrometry using two methods: thermal ionization mass spectrometry (TIMS) and multi collector inductively coupled plasma mass spectrometry (MC-ICPMS). The results are given in the δ notation described in equations (1) and (2) with the secular equilibrium between $^{234}U/^{238}U$ as a 'standard'. Refer to *Scholz and Hoffmann* [2008] and *Fensterer* [2011] for a detailed description on the U-series methods.

At least 200 mg of sclerosponge sample were sent to the University of Heidelberg for dating by the U-series disequilibrium methods. Chemical preparation of the samples follows the guidelines described in the Appendix of *Scholz et al.* [2004] for TIMS. The sponges were determined to be closed systems with the $\delta^{234}U$ values for each dating sample being within 10‰ of the modern seawater ratio of 150‰ [*Scholz et al.*, 2004]. Table 1 summarizes the results obtained.

Table 1. Results of the uranium-thorium analysis

Sample ID	$\delta^{234}U$ (‰)	^{238}U (µg/g)	^{232}Th (ng/g)[a]	^{230}Th (pg/g)	Age (cal yr)	Distance (cm[b])
LP47-1-0,8	149.8 ±1.9	7.6734 ±7.7E-3	7.173 ±6.3E-2	0.1042 ±4.2E-3	1953.5 ±12	0.8
LP47-1-1,1	146.9 ±1.6	7.5622 ±7.6E-3	6.459 ±6.5E-2	0.133 ±1.0E-2	1928 ±13.2	1.1
LP47-1-2,1	145.2 ±1.6	7.5373 ±7.5E-3	5.672 ±3.1E-2	0.1532 ±8.3E-3	1909.4 ±11.3	2.1
LP47-1-3,1	144.6 ±1.7	7.4845 ±7.5E-3	5.331 ±5.2E-2	0.228 ±1.2E-2	1849.4 ±13.05	3.1
LP47-1-4,1	142.5 ±1.7	7.4771 ±7.5E-3	5.178 ±5.7E-2	0.274 ±2.1E-2	1812.1 ±18.15	4.1
LP47-1-4,4	148.0 ±2.0	7.3893 ±7.4E-3	5.066 ±2.5E-2	0.2634 ±7.1E-3	1818.8 ±10.2	4.4
LP47-1-B	157.5 ±1.6	7.3712 ±7.4E-3	4.917 ±3.9E-2	0.4221 ±6.8E-3	1695 ±10	9.5
LP36-1-1,2	152.2 ±2.1	7.7260 ±7.7E-3	5.431 ±4.1E-2	0.0834 ±2.7E-3	1964 ±9	0.8
LP36-1-0,91	141.7 ±1.8	7.6945 ±7.7E-3	5.984 ±6.0E-2	0.0744 ±8.6E-3	1972.1 ±11.7	0.91
LP36-1-1,9	143.2 ±1.8	7.6075 ±7.6E-3	4.660 ±3.2E-2	0.1395 ±9.6E-3	1917.4 ±10.7	1.9
LP36-1-2,9	144.4 ±1.7	7.6012 ±7.6E-3	4.405 ±3.7E-2	0.179 ±1.9E-2	1886.4 ±16.1	2.9
LP36-1-4,1	144.5 ±1.6	7.5667 ±7.6E-3	3.824 ±1.9E-2	0.1852 ±9.4E-3	1879 ±9.85	4.1
LP36-1-B	148.8 ±2.1	7.4076 ±7.4E-3	4.163 ±3.2E-2	0.2131 ±7.2E-3	1855.8 ±8.95	7.5
CB69-1	149.7 ±2.8	7.6662 ±8.4E-3	4.097 ±1.4E-2	0.1482 ±3.9E-3	1913.1 ±7.2	1.3
CB69-2	142.3 ±2.2	7.5822 ±7.6E-3	6.903 ±4.3E-2	0.2232 ±8.5E-3	1862.9 ±13.3	2.5
CB69-3	148.7 ±2.5	7.5266 ±7.5E-3	3.958 ±1.6E-2	0.2673 ±6.9E-3	1818.8 ±8.45	3.7

[a] Concentrations are in agreement with previously published results for the top 200m of eastern Caribbean Sea[*Huh and Bacon*, 1985].

[b] Distances are measured from the surface of the sponge along the growth axis.

The age models (Figure 3) for the specimens collected from La Parguera at 36 and 47 m (LP 36 and LP 47) are based on six and seven U/Th dates, respectively, and the collection date. The age model for our Cane Bay specimen (CB 69) was based on three U/Th dates plus the collection date. The best fit through the dating points for each specimen was a weighted 3rd degree polynomial model for LP 36, a weighted exponential age model for LP 47 and a weighted 2nd degree polynomial model for CB 69. The U/Th age models show that the LP 36, LP 47 and CB 69 had records of length 220yr (1776-1995), 464yr (1532-1995) and 167yr (1829-1995) respectively. $\delta^{13}C$ from each of the sponges was used to validate each age models. $\delta^{13}C$ curves from all three sclerosponges behave similar to the well-known and dated carbon

enrichment curves [*Swart et al.*, 2010]. One can use the curve to get a general age model of the last 200 years. The age models suggest an average growth rate of 181.5µm/yr for LP 36, 146.4µm/yr for LP 47 and 181.8µm/yr for CB 69, all within previously published growth rates for *C. nicholsoni* of between 100–300µm/yr [*Swart et al.*, 1998, 2002; *Böhm et al.*, 2000; *Lazareth et al.*, 2000; *Haase-Schramm et al.*, 2003; *Rosenheim et al.*, 2005].

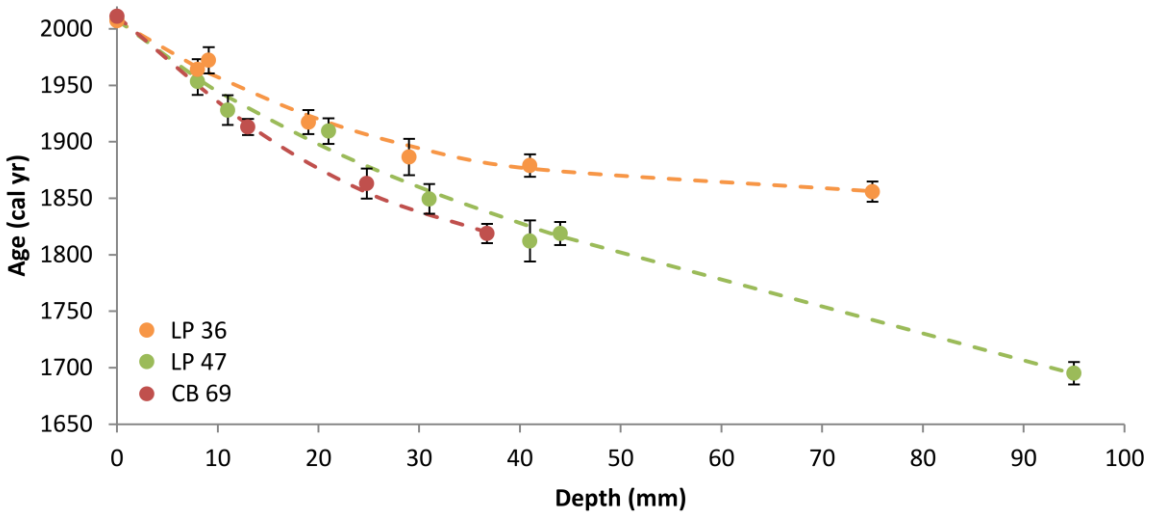

Figure 3 U/Th dating results with the corresponding age models for each sclerosponge. The model for LP 36 is A = (-3.7E-13 ± 1.0E-12) d^3 + (7.8E-8 ± 1.0E-7) d^2 - (5.8E-3 ± 2.3E-3) d +2007, LP 47 uses A = (101.9 ± 169.2) exp((-4.9 ± 9.8E-5) d) + (1906 ± 169) exp((-1.2E-6 ± 9.4E-7) d) and CB 69 uses the model A = (9.1E-8 ± 2.0E-7) d^2 - (8.5E-3 ± 6.7E-3) d + 2011 where A is the age in calendar years and d is the distance from the sclerosponge surface measured in micrometers.

By using the individual age models for each sponge just mentioned sampling depth was converted to the time domain and then MATLAB was applied to perform a spline function to the stable isotope date which resampled the sub-annual results to annual resolution.

3. Results

3.1 Oxygen isotopes

Figure 4 shows the annualized stable isotope results for the three sponges using the age models described above. Three distinct phases according to the long-term trends and average values were observed in the annual $\delta^{18}O_{arag}$ of the sclerosponges. Phase I encompasses the time interval from 1532 to 1756, phase II extends from 1764 to 1827 and phase III starts in 1854 and ends in 1995. The transitional period from phase II to phase III and phase III in its entirety is the only interval when all three sponge records occur together. Generally the lowest

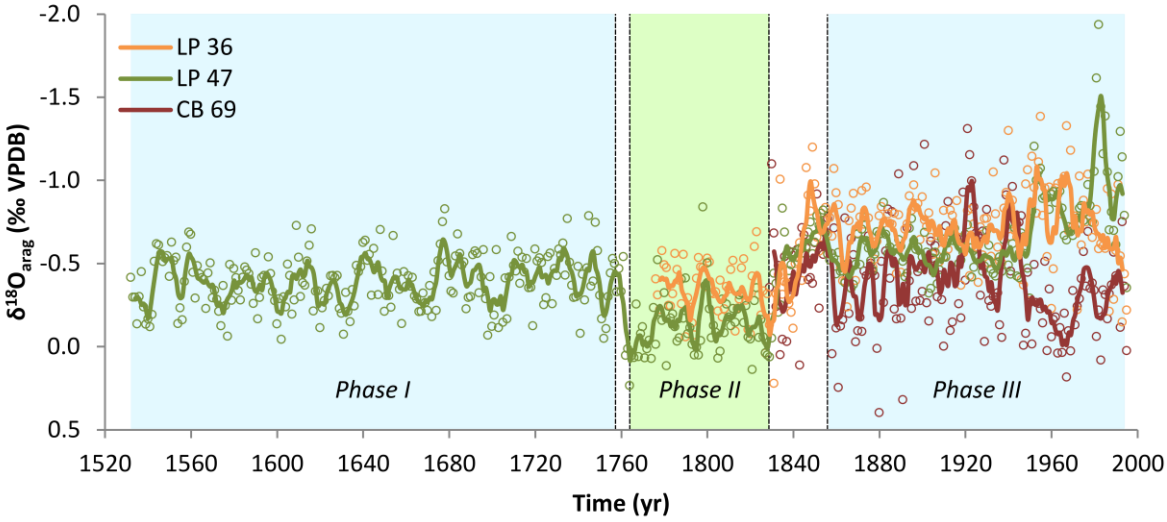

Figure 4 $\delta^{18}O_{arag}$ values obtained from the sponges. Circles denote the annual values resampled from sub-annual resolution. Solid lines represent 5-year running averages. Highlights show phases I through III (see text).

sclerosponge in the mixed layer (CB69) has the heaviest (colder) isotope ratios while the highest sponge (LP 36) in the water had the lightest (warmer) values.

LP 47, the longest record, shows an average $\delta^{18}O_{arag}$ of -0.39‰ (VPDB) with a slight negative trend during phase I. Phase II shows consistently more positive $\delta^{18}O_{arag}$ values with an average of -0.13‰ (VPDB). Phase III presents a more negative trend and the most negative

$\delta^{18}O_{arag}$ overall with an average value of -0.67‰ (VPDB). Between phase I and phase II there is a transitional interval of 8 year that shows a positive trend of 0.09‰ yr^{-1} while the 27 year-long transitional period from phase II to phase III shows a negative trend of 0.03‰ yr^{-1}. The total amplitude for the complete LP 47 record is 2.17‰ (VPDB).

The annual record derived from LP 36 starts during phase II with an average $\delta^{18}O_{arag}$ value of -0.34‰ (VPDB). Phase III shows a negative trend in the $\delta^{18}O_{arag}$ values with an average of -0.72‰ (VPDB), more than twice as negative of that of phase II. Like LP 47, the 27 year-long transitional period between phase II and III has the same decrease in the oxygen ratio of -0.03‰ yr^{-1}. The amplitude between the highest and lowest isotope ratios for the complete record is 1.61‰ (VPDB).

The stable isotope ratios of the shortest annual record, CB 69, start during the transitional period between phase II and III (1829) but it shows a sub-division beginning in 1945 lasting until the end of the record. The $\delta^{18}O_{arag}$ curve shows a slight negative trend before this division and has an average value of -0.46‰ (VPDB). After 1945 the $\delta^{18}O_{arag}$ curve shows a somewhat sudden change to more positive values with an average value of -0.26‰ (VPDB). The difference between the highest and lowest oxygen isotope ratios for the complete record is 1.71‰ (VPDB). The $\delta^{18}O_{arag}$ values from CB 69 also show greater variance than the other two sponges from 1829 to 1995 (0.10‰^{2} for CB 69 vs. 0.06‰^{2} for LP 47 and 0.07‰^{2} for LP 36).

3.2 Carbon isotopes

All three sponges show the "Suess effect" which manifests itself as a decrease in $\delta^{13}C$ values (Figure 5). Specimen LP 47 shows an average rate of decrease of -0.011‰ yr^{-1} (VPDB) in the period from 1900 to 1990 and -0.022‰ yr^{-1} (VPDB) from 1960 to 1990. LP 36 and CB 69 show the same decrease rate for the 1900 to 1990 of -0.007‰ yr^{-1} (VPDB) and an exceptionally similar decrease rate of -0.015‰ yr^{-1} (LP 36) and -0.017‰ yr^{-1} (CB 69) from 1960 to 1990. These results are in very good agreement with those compiled by *Swart et al.* [2010]. They reported an average decrease rate in coral $\delta^{13}C$ values of -0.0085‰ yr^{-1} and -0.019‰ yr^{-1} (VPDB) for the time intervals of 1900 to 1992 and 1960 to 1990, respectively, in the Atlantic Ocean. *Swart et al.* [2010] also found a $\delta^{13}C$ mean change in sclerosponge values of -0.01‰ yr^{-1} and -0.0093‰ yr^{-1} (VPDB) for the Caribbean and the Bahamas, respectively, for the period of 1900 to 1990.

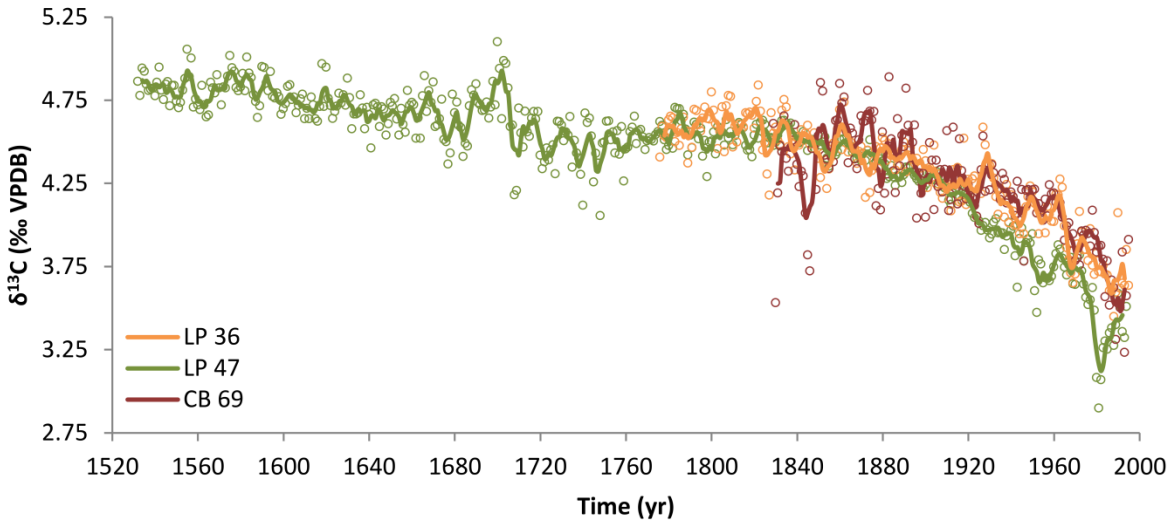

Figure 5 $\delta^{13}C$ obtained from the sponges. Circles denote the annual values resampled from sub-annual resolution. Solid lines represent 5-year running averages. The isotopes from all three sponges show the depletion of ^{13}C in the oceans since the mid-1700, the Suess Effect.

3.3 Temperature calibration

It is well known that the oxygen stable isotope ratios contained in the calcium carbonate of marine organisms are dependent on the ocean temperature and the salinity of the water in which the organisms precipitated their aragonite. Present seasonal salinity range in our study region is 1.22PSU from 0 to 30m that is controlled, in part, by the Orinoco River discharge which can be measured in the northeastern Caribbean for a short duration in October [*Antonov*

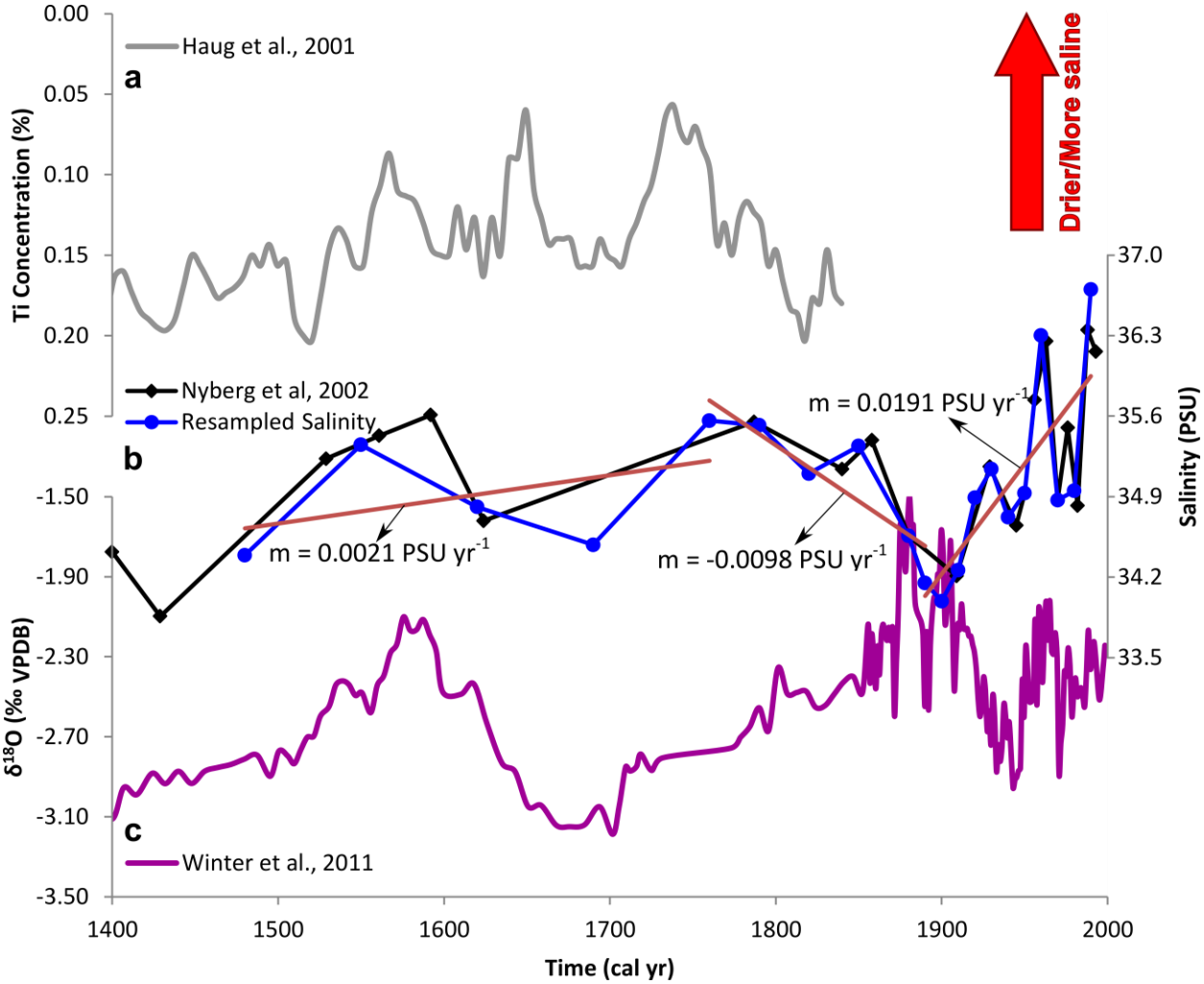

Figure 6 Effects of the Orinoco river discharge and precipitation on the Caribbean salinity. Long term salinity changes in the northeastern Caribbean a due, in part, to changes in the Orinoco river discharge, reconstructed in (a) by Ti concentrations in the Cariaco Basin sediments and by precipitation changes, reconstructed in (c) from a Puerto Rican speleothem. The long term trend of the reconstructed salinity in (b) (black) is in good agreement with both the Orinoco discharge and the precipitation patterns discovered with the Puerto Rican speleothem except in the late 19th century. (b) shows the resampled salinity using MATLAB (blue, see text) and the salinity rates sincethe late 15th century (red).

et al., 2010]. However, these changes become more subtle with increasing depth and are controlled by long term precipitation changes over the northeastern Caribbean (Figure 6c) and long term Orinoco River discharge (Figure 6a) [*Haug et al.*, 2001; *Nyberg et al.*, 2002; *Antonov et al.*, 2010; *Winter et al.*, 2011].

The only available Caribbean salinity reconstruction was used for the period from 1400 to 1993 AD [*Nyberg et al.*, 2002] (Figure 6b black) to remove the effect of salinity on the sclerosponge $\delta^{18}O$ record. This reconstruction has a salinity range of 2.49PSU and was divided into three sections that show distinct temporal resolutions (1400–1624, 1787–1880, 1909–1993). Because the *Nyberg et al.* [2002] reconstruction is not spaced evenly, the data was resampled using a spline function through the average temporal resolution of each section using MATLAB (Figure 6b blue). This curve could now be divided into three sections with clearly distinct linear trends (1480–1760, 1760–1890, 1890–1990). From 1990 to the 2000 salinity values for 36 m, 47 m and 69 m were available from the World Ocean Atlas 2009 [*Antonov et al.*, 2010].

Salinity values (calculated and observed) were converted into $\delta^{18}O_{water}$ (VSMOW) using the relation between salinity and $\delta^{18}O_{water}$ for the northeastern Caribbean upper surface waters derived from *Schimdt et al.*, [1999] (Figure 7a):

$$\delta^{18}O_{water}\ (VSMOW) = 0.2943\ (\pm 0.0621)\ S - 9.639\ (\pm 2.21) \qquad (6)$$

The resulting $\delta^{18}O_{water}$ was then subtracted from the $\delta^{18}O$ from the sclerosponges ($\delta^{18}O_{arag}$) [$\delta^{18}O_{arag} - \delta^{18}O_{water} = \delta^{18}O_T$] resulting in $\delta^{18}O_T$ a more precise recorder of temperature. The student-researcher calibrated $\delta^{18}O_T$ from all three sponges against the northeastern Caribbean region (17-19°N, 63-69°W) temperature reconstruction from NOAA's ERSSTv3b (1854 to

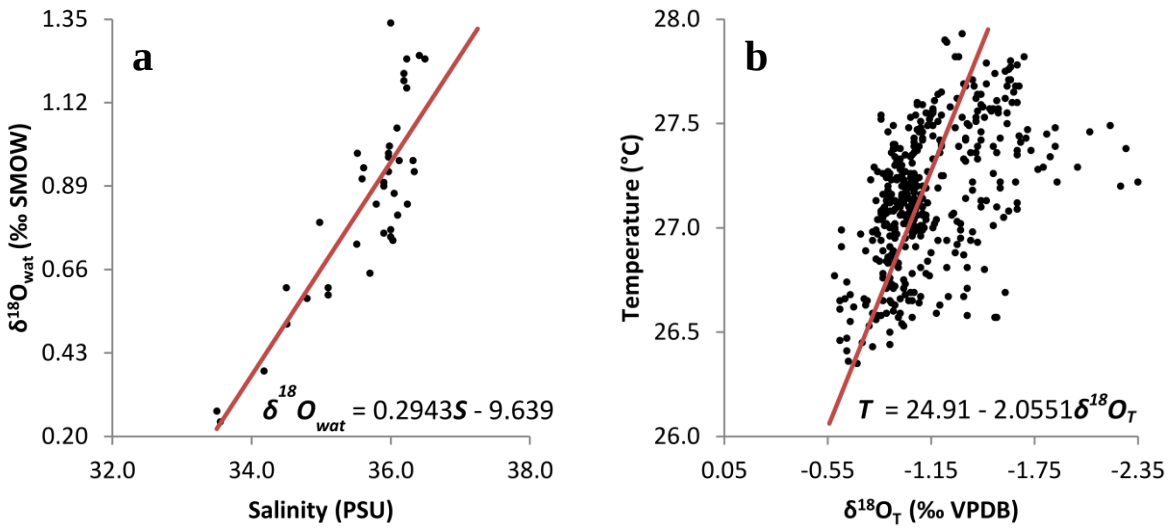

Figure 7 (a) Modern linear relation between Caribbean surface water salinity and their $\delta^{18}O$. (b) Linear relation between $\delta^{18}O_T$ (see text) and gridded temperature from the ERSSTv3b. The relationship was obtained by smoothing the $\delta^{18}O_T$ series with a 5-year running average and using the robust least-squares method that reduces the effect of outliers over the regression.

present, Figure 7b). The ERSSTv3b uses historical surface observations and statistical methods to provide gridded data [*Smith et al.*, 2008]. Temperatures at depth were obtained by interpolating the surface temperatures using the modern Caribbean temperature profile [*Locarnini et al.*, 2010]. Calibrating the $\delta^{18}O_T$ data against gridded SST implies that an important part of the temperature signal recorded by the specimens is related to open-ocean conditions. A least squares linear regression was used on a $\delta^{18}O_T$ ($\pm 2\sigma$) vs. SST plot after smoothing with a 5 year average to account for high frequency, likely local, changes in the $\delta^{18}O_T$ values:

$$\delta^{18}O_T = \ 13.14\ (\pm 2.245) - [0.5252\ (\pm 0.08245)]SST(°C) \qquad (7)$$

with n = 414 and r^2 = 0.2758. The regression improves by 98% after applying a robust fit using the bisquare weights method which reduces the effects of outliers over the least squares linear regression method:

$$\delta^{18}O_T = 12.12\ (\pm 1.775) - [0.4866\ (\pm 0.0653)]SST(°C) \quad (8)$$

(n = 414, r^2 = 0.5457). Solving equation 8 gives us the final SST/$\delta^{18}O_T$ used in this study:

$$SST\ (°C) = 24.91\ (\pm 6.99) - [2.0551\ (\pm 0.2758)]\delta^{18}O_T \quad (9)$$

3.4 Temperature reconstruction

Figure 8 shows the sclerosponge-derived temperature results using the methods described above. As expected, the coldest temperatures were obtained from the sponge deepest in the mixed layer (CB 69) while the warmer temperatures were from the sponge highest in the water column (LP 36). The coldest temperatures for the entire period of study (1532 to 1995) were recorded in phase II. LP 47 and LP 36 consistently recorded the coldest temperatures during phase II. Starting near the beginning of phase II, the LP 36-derived $\delta^{18}O_T$ record shows a slightly more negative average value that LP 47 during phase II (-0.82‰ vs. -0.74‰; equivalent to 26.6°C and 26.4°C, respectively). If the salinity effects had not been the slopes of derived SSTs taken solely from $\delta^{18}O_{arag}$ would have been much lower. This is noticeable

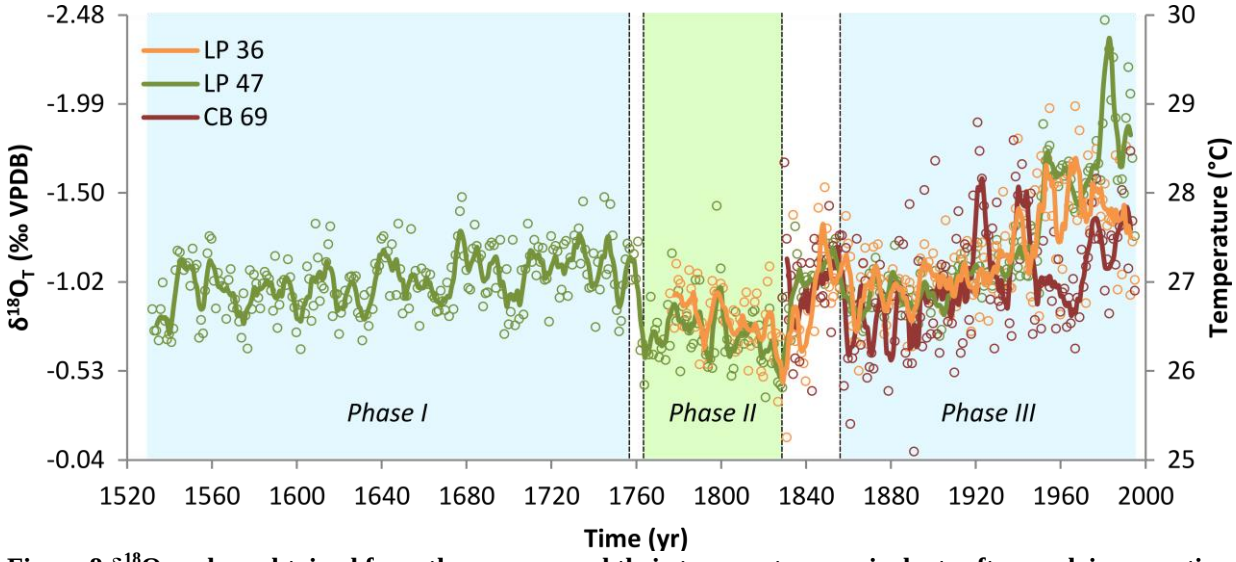

Figure 8 $\delta^{18}O_T$ values obtained from the sponges and their temperature equivalents after applying equation 9. Circles denote the annual values resampled from sub-annual resolution. Solid lines represent 5-year running averages. Highlights show phases I through III (see text).

primarily in phase III for all three sponges. Here the $\delta^{18}O_T$ ratios of LP 47 show a linear trend of -0.008‰ yr^{-1} (0.016°C yr^{-1}), more than twice its linear $\delta^{18}O_{arag}$ trend (-0.003‰ yr^{-1}). The $\delta^{18}O_T$ slope for LP 36 is -0.0042‰ yr^{-1} (0.0087°C yr^{-1}) and negligible for $\delta^{18}O_{arag}$. The $\delta^{18}O_T$ slope for CB 69 is -0.0032‰ yr^{-1} (0.0066°C yr^{-1}) and 0.0010‰ yr^{-1} for $\delta^{18}O_{arag}$. The average $\delta^{18}O_T$ values for LP 47 and LP 36 during phase III were -1.21‰ (27.4°C), and -1.16‰ (27.3°C) respectively.

The transitional period for LP 47 between phases I and II and phases II and III shows temperature-change rates of -0.18°C yr^{-1} and 0.045°C yr^{-1}, respectively. For the entire record, LP 47 shows a $\delta^{18}O_T$ range of 2.39‰ (4.91°C). The $\delta^{18}O_T$ difference between the highest and lowest points found in LP 36 is 1.81‰ (3.72°C). The 27 year-long period connecting phase II and III shows an increasing temperature-change rate of 0.050°C yr^{-1}, very similar to that of LP 47. The maximum range of $\delta^{18}O_T$ in CB 69 was 1.86‰ (3.8°C). A small change in average temperature occurred from 1829-1945 and 1945-present: the first section shows an average $\delta^{18}O_T$ of -0.96‰ (26.9°C) while the second section indicates an average $\delta^{18}O_T$ of -1.11‰ (27.2°C). A sudden drop of temperatures for CB 69 at ~1945 and the beginning and subsequent sudden rise at ~1960 is probably the result of a rise in the mixed layer depth, submerging CB 69 in colder, temperature-stable waters during this period. Although the $\delta^{18}O_{arag}$ variance in the CB 69 record is higher than that from LP 47 and LP 36, the temperature variance for the 1829–1995 period of all three sclerosponge records is very similar (LP 47: 0.59°C^2, LP 36: 0.42°C^2, CB 69: 0.47°C^2). A possible explanation for this is the greater salinity fluctuations in shallower waters [*Antonov et al.*, 2010].

3.5 Spectral analysis

The sclerosponge derived temperature data was first processed using a binomial low-pass filter using MATLAB to reduce the influence of higher frequencies and possible local effects. A continuous wavelet analysis was then performed using PAST software [*Hammer et al.*, 2001]. A lag-1 (red noise) coefficient [*Torrence and Compo*, 1998] of 0.917 was used for LP 36, 0.955 for LP 47 and 0.790 for CB 69. Red noise has long been correlated to climatic signals [*Hasselmann*, 1976]. Spectral analysis of LP 36 revealed two intervals with significant (chi-squared, 95% confidence) results (1826-1865 and 1943-1973; Figure 9a) that show strong decadal variability and a few other shorter intervals with sub-decadal variability. The wavelet analysis for LP 47 shows two significant (chi-squared, 95% confidence) time intervals with decadal variability (1735-1770 and 1783-1807) similar to LP 36 as well as other shorter intervals of sub-decadal variability. Applying a five point moving average filter instead of a

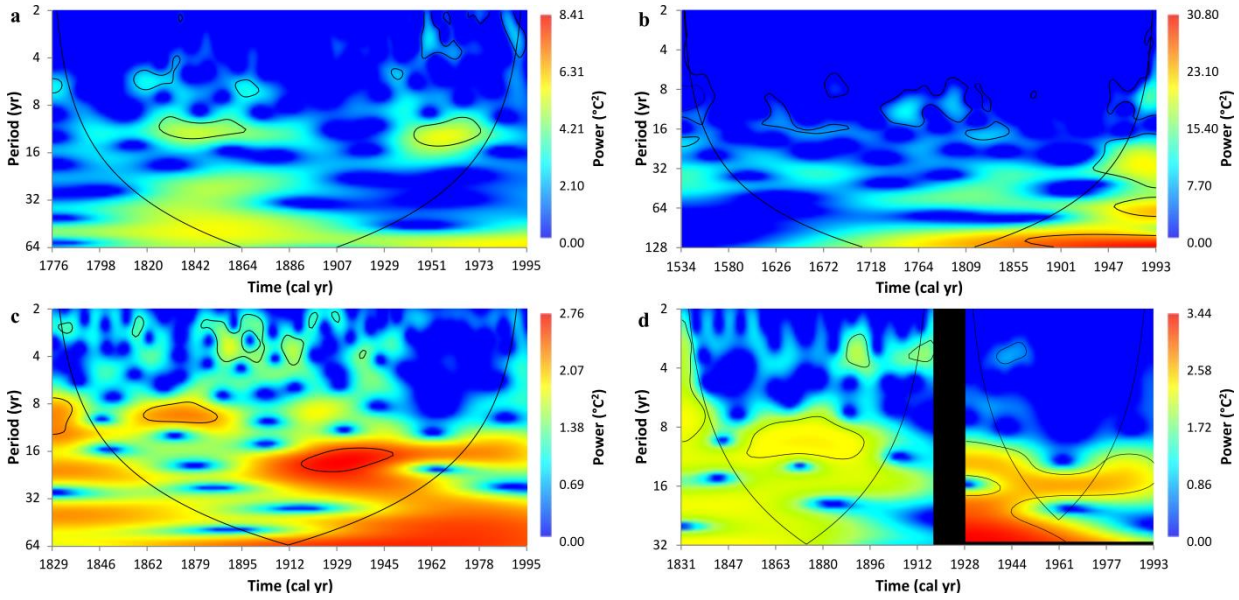

Figure 9 Wavelet plots of the sclerosponge-derived temperatures. The LP 36 wavelet (a) shows two continuous time intervals with strong decadal variability, LP 47 (b) shows seven such intervals. The original wavelet of CB 69 (c) two intervals with strong decadal variability and one interval with multidecadal variability but this last interval was determined to be the artifice of a few outliers. (d) shows the composite wavelet of CB 69 after the removal of the outliers which shows four intervals of strong decadal variability. All outlined intervals (a-d) are in the 95% confidence levels. The cone of influence is shown for all plots.

binomial low-pass filter to the LP 47 temperature time series, however, produced a wavelet plot that shows seven time intervals with significant decadal variability (1532-1566, 1613-1640, 1727-1766, 1781-1814, 1825-1833, 1946-1954 and 1972-1995) (Figure 9b). A moving average filter has the advantage of removing the higher frequency variability without introducing artificial bias [*Smith*, 1997].

The wavelet analysis for the binomially filtered CB 69 resulted in two significant (chi-squared, 95% confidence) time intervals of decadal variability (1829-1835 and 1861-1886) and one time interval with strong quasi-multidecadal variability from 1917 to 1948. Other intervals also resulted showing sub-decadal variability (Figure 9c). The quasi-multidecadal intervals in CB69 are probably the result of six outliers interacting with the surrounding data points that alter the wavelet analysis. Performing a wavelet analysis on two individual sections of the CB 69 without the six outliers, this time using a 5 point moving average similar to LP 47 and using a red noise coefficient of 0.754 for the first section and 0.915 for the second section [*Torrence and Compo*, 1998] clearly showed four time intervals with strong decadal variability (1829-1835, 1854-1893, 1929-1952 and 1974-1993, chi-squared, 95% confidence) (Figure 9d), three intervals with significant sub-decadal variability and one period with significant quasi-multidecadal variability.

4. Discussion

The temperature reconstructions from the two shallower sponges indicate an increase of 1.13°C (LP 36) and 1.80°C (LP 47) in average temperature over 200 years from the coldest temperatures recorded in the Little Ice Age to the 20th century. Although all three sponges show very similar average temperatures dominating the mid-19th century (Figure 8, Phase III) (LP 47:

26.89°C; LP 36: 26.82°C; CB 69: 26.80°C), CB 69 shows a much smaller temperature increase over the last 150 years (0.40°C) than LP 47 (1.51°C) and LP 36 (1.02°C). This smaller increase in CB 69's temperature is expected as it lived near the bottom of the modern mixed layer [*Kara et al.,* 2000; *Locarnini et al.,* 2010] where the temperature is affected by the fluctuating up/down movement of the mixed layer depth so the sponge is constantly dipping below and resurfacing above the thermocline. This is evidenced by the variability found in the CB 69 record (Section 3.1).

For the period 1950 to 1995 LP 36 and LP 47 temperature profiles diverge. LP 36 shows decreasing temperature while LP 47 increases but both show similar temperatures for the last part of the record. This apparent inconsistency can be explained by the uncertainty of the temperature calibration used (Section 3.3) and/or by heat dynamics in the water column: the water mass at 36m would need a smaller temperature increase to achieve temperature equilibrium with shallower waters than the water mass 47m deep.

The results discussed here are very similar to other Caribbean SST reconstructions obtained from sclerosponges located in the Pedro Bank, Jamaica [*Haase-Schramm et al.,* 2003] (Figure 10c); corals off Puerto Rico [*Kilbourne et al.,* 2008] (Figure 10a) and foraminifera from the Cariaco trench [*Black et al.,* 2007] (Figure 10b) and the Gulf of Mexico [*Richey et al.,* 2007] (Figure 10d). All these records of reconstructed Caribbean SST show an increase of 1.08 to 2.18°C from the second half of the 18th century to that of the second half of the 20th century except for *Black et al.* [2007] which shows an increase of only 0.20 °C. The lower amplitude of the *Black et al.* [2007] record is probably a result of the Cariaco Basin situated in an area of seasonal upwelling that has an important control over the annual temperature range. The

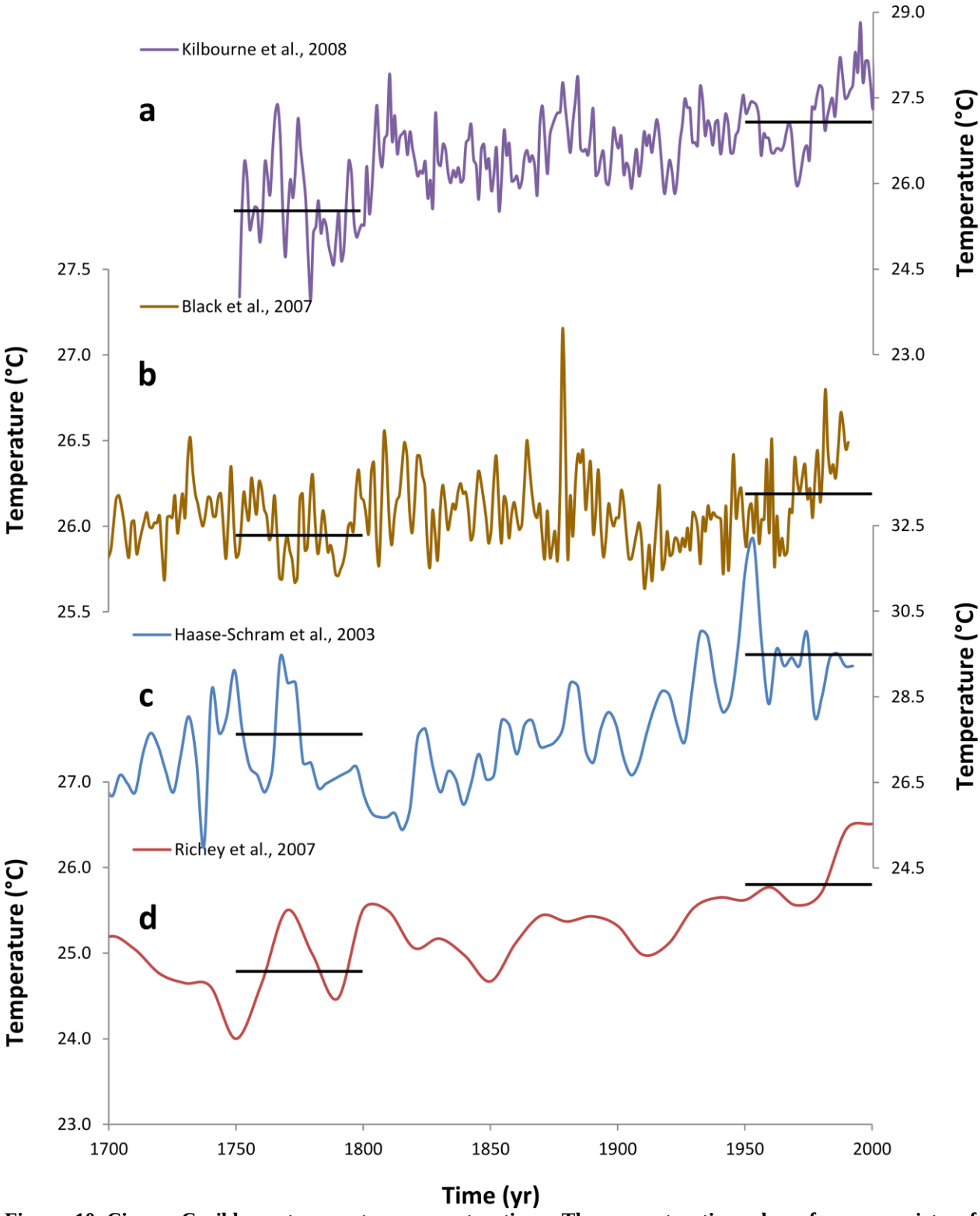

Figure 10 Circum-Caribbean temperature reconstructions. The reconstructions done from a variety of proxies (a corals; b foraminifera, c sclerosponge and d with warm species foraminifera using the *Regenberg et al.* [2009] calibration). The black lines over the curve represent the average temperature from 1750-1800 and 1950-2000. Every record shows a rise in average temperatures from 0.20°C (b) to 2.18°C (c).

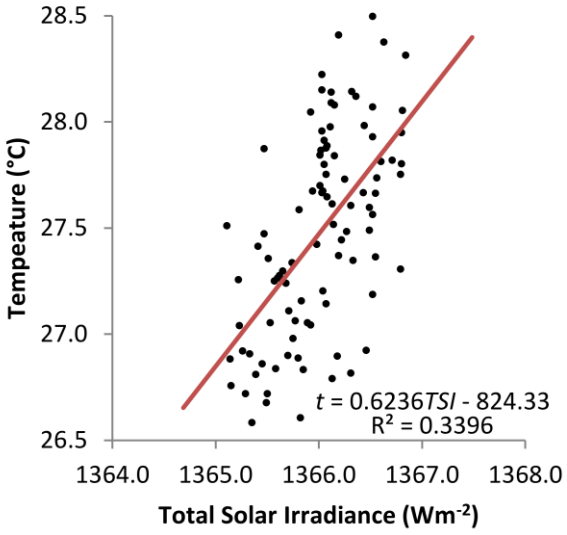

Figure 11 First approximation of Caribbean Sea temperature sensitivity to solar changes for the 20th century. Total solar irradiance Changes in solar activity were able to explain 34% of the average, sclerosponge-derived, temperature variability of the water column in the northeastern Caribbean during the 20th century. The slope of the linear regression represents the solar climate sensitivity, 0.62 °C/Wm^{-2}.

Kilbourne et al. [2008] coral record, located ~5.75 km from LP 36 and LP 47, shows a long term linear temperature trend from the mid-18th century to the present (0.0072 °C yr^{-1}) which is nearly identical to that derived from LP 36 and LP 47 (0.0067 °C yr^{-1} and 0.0081 °C yr^{-1} respectively). This supports the results of our temperature calibration and age models applied on this research.

This rise in temperature is similar to recent model estimates primarily when solar forcings are used as input [*Delworth and Knutson*, 2000; *Shindell et al.*, 2001; *Waple et al.*, 2002; *Meehl et al.*, 2003; *Ammann et al.*, 2007]. Solar variability is seen as a common component in many temperature reconstructions [*Hong et al.*, 2000; *Hai et al.*, 2002; *Haase-Schramm et al.*, 2003; *Jiang et al.*, 2005; *Richey et al.*, 2007]. The sclersopsonge SST reconstructions were compared to *Lean's* [2000] total solar irradiance (TSI) for the period 1776 to 1995 (after reducing its amplitude by 25% so it would agree with more modern TSI reconstructions [*Lean et al.*, 2002; *Vieira et al.*, 2011]). The cross correlation coefficient is 0.68 (t-test, $p << 0.01$) for LP 36 and 0.76 (t-test, $p << 0.01$) for LP 47. When comparing the entire record of LP 47 to the entire TSI

reconstruction (1610-1995), the cross correlation coefficient decreased somewhat to 0.45 (t-test, p << 0.01). The CB 69 record (1829 -1995) also shows a strong correlation to TSI (0.50; t-test, p << 0.01). The average annual reconstructed sea temperature of the mixed layer (average temperature calculated using the annual temperature from each sponge) for the 20th century was regressed to TSI and a slope of 0.62 °C/Wm^{-2} was obtained (Figure 11). This result supports the

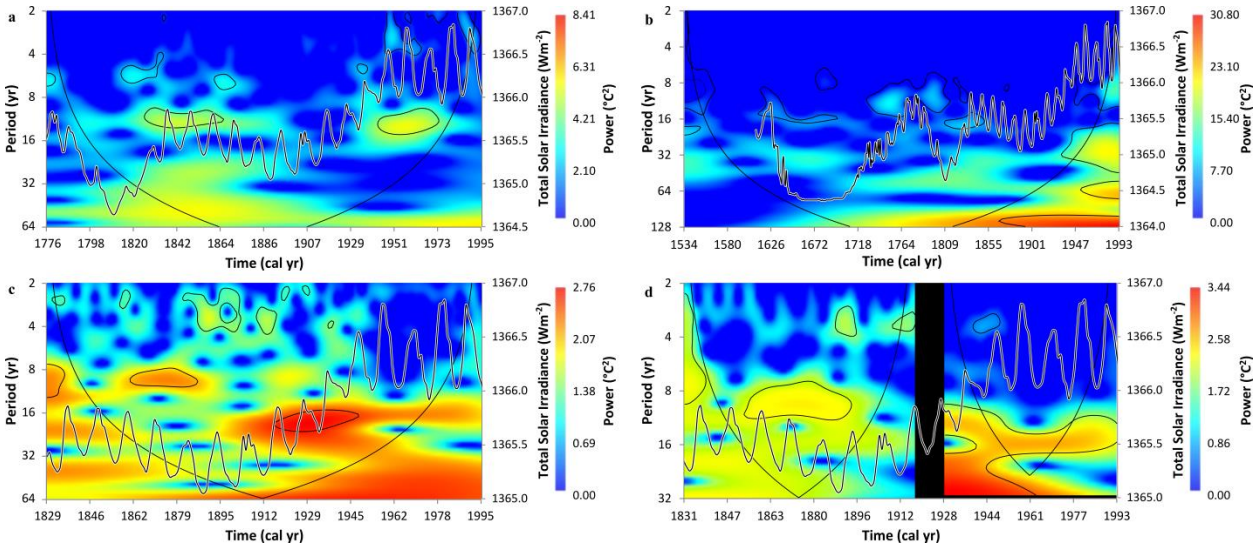

Figure 12 *Lean's* [2000] total solar irradiance superimposed over the sclerosponge-derived temperature wavelet plots after reducing its amplitude by 25%. The intervals of strong decadal variance are in good synchronicity with the lower frequency changes in TSI, especially LP 36 (a) and LP 47 (b).

satellite data-derived calculation of *Douglass and Clader* [2002] for solar climate sensitivity for the 1970-2000 period (0.63 K/Wm^{-2}). This remarkable similarity implies that solar irradiance is likely forcing long-term Caribbean SST variability and that sclerosponges are sensitive recorders of subtle changes in ambient water temperature.

Figure 12 shows the TSI curves just discussed superimposed on the wavelet plots (see Figure 9). Comparing both these records strongly suggests a quasi SST-TSI coupling. When the TSI goes above a threshold value of 1365.20Wm^{-2} the result is significant decadal variability in SSTs. If the periods of significant decadal variability seen in our SST reconstructions result

from higher solar activity there should be a strong correlation between the strength of the 11-year solar cycle and the temperature reconstructions at those periods (decadal variability ON) and a weaker correlation when the decadal variability is not significant (decadal variability OFF) with

Table 2 Comparisons between the sclerosponge-derived temperatures to the total solar irradiance after removing the multidecadal trends from the temperature series

LP 47					CB 69					LP 36				
I[a]	DV[b]	SCC[c]	Lag (yr)[d]	p[e]	I[a]	DV[b]	SCC[c]	Lag (yr)[d]	p[e]	I[a]	DV[b]	SCC[c]	Lag (yr)[d]	p[e]
1532-1566[f]	ON	NA	NA	NA	1829-1835	ON	0.77	0	<0.05	1776-1825	OFF	0.19	3	>0.10
1567-1612[f]	OFF	NA	NA	NA	1836-1853	OFF	0.41	10	>0.10	1826-1865	ON	0.39	2	<0.05
1613-1640	ON	0.55	9	<0.05	1854-1893	ON	0.41	7	<0.05	1866-1942	OFF	0.07	3	>0.10
1641-1726	OFF	0.27	4	<0.05	1894-1917	OFF	0.27	5	>0.10	1943-1973	ON	0.36	5	<0.10
1727-1766	ON	0.51	4	<0.05	1918-1928	NA	NA	NA	NA	1974-1995	OFF	0.18	3	>0.10
1767-1780	OFF	0.47	4	>0.10	1929-1952	ON	0.40	10	>0.10					
1781-1814	ON	0.34	4	<0.10	1953-1973	OFF	0.22	4	>0.10					
1815-1824	OFF	0.84	4	<0.05	1974-1993	ON	0.56	4	<0.05					
1825-1833	ON	0.46	2	>0.10										
1834-1945	OFF	0.20	0	<0.05										
1946-1954	ON	0.78	4	>0.10										
1955-1971	OFF	0.20	5	>0.10										
1972-1995	ON	0.48	8	<0.10										

[a] Time interval
[b] Decadal variability as obtained from the wavelet analysis of temperature
[c] Solar cycle correlation to temperature
[d] Lag used to obtain the maximum correlation
[e] Cross-correlation significance represented by the p value
[f] The comparison between the temperature reconstruction and the solar cycle could not be done in these intervals due to the fact that the *Lean* [2000] reconstruction begins in the year 1610.

a lag not greater than 10 years to account for the time for radiative equilibrium to be achieved within the mixed layer [*White et al.*, 1997] and small uncertainties in our age model. The hypothesis was tested by removing the multidecadal trend from the temperature reconstructions and calculating the cross-correlation between each individual sclerosponge temperature reconstruction and the 11-year solar cycle [*Lean*, 2000]. This was a successful test, as summarized in Table 2, as it was possible to attribute more than 35% of the decadal variability in the temperature records to changes in solar activity in every case but one with confidence levels

better than 90% (t-test) in every case but three. These results indicate that the Caribbean Sea is responding to high frequency changes in solar forcing. The results give more importance to the 11-year solar cycle than the results by *Dima et al.* [2005] who determined that the solar cycle only explains 8% of the temperature variability analyzed from a number of sources (gridded and proxy-derived temperature, historical observations) using the principal oscillation pattern analysis and 14% using empirical orthogonal functions. A possible explanation of this discrepancy is that *Dima et al.* [2005] used continuous time intervals for their analysis while the discrete intervals chosen according to the low frequency changes in TSI were used in this study.

The results from all three sponges set the hypostatized TSI threshold at an average value of 1365.29Wm^{-2} (max 1365.80Wm^{-2}, min 1364.65Wm^{-2}) from the early 15th century to the first half of the 20th century. The second half of the 20th century presents a second average threshold of 1366.12Wm^{-2} (max 1366.33Wm^{-2}, min 1365.94Wm^{-2}). The latter threshold might differ in nature from the former due to anthropogenic influences to global warming becoming more important in the second half of the 20th century [*Tett et al.*, 1999; *Delworth and Knutson*, 2000; *Barnett et al.*, 2001; *Meehl et al.*, 2003].

5. Conclusions

At the time of collection, the sclerosponges were recording open Northeastern Caribbean Sea temperatures. The temperature reconstruction from each sponge shows an increase in average temperature from the 19th to the 20th century that is in agreement with other reconstructions from the Circum-Caribbean region. Although the temperature increase from the deeper sponge is 41-74% smaller than our shallower ones, it is a significant one. This can probably be interpreted as an expansion of the mixed layer in our study area.

The temperature reconstructions indicate that an important driving mechanism for long term temperature trends is solar forcing which explains at least 45% and as much as 76% of the observed variability. The results show a first-approximation climate sensitivity of 0.62°C/Wm^{-2} to solar forcing for the 20th century in near exact agreement with previously published work. Furthermore, the results suggest a TSI threshold that needs to be surpassed to explain the decadal variability in the records. This threshold was determined to have an average value 1365.29 Wm^{-2} until the first half of the 20th century. Once the threshold was reached, TSI was able to explain more than 35% of the decadal variability observed in our records. More work is needed to fully confirm this hypothesis.

6. References

Ammann, C. M., F. Joos, D. S. Schimel, B. L. Otto-Bliesner, and R. A. Tomas (2007), Solar influence on climate during the past millennium: results from transient simulations with the NCAR Climate System Model., *Proceedings of the National Academy of Sciences of the United States of America*, *104*(10), 3713–8, doi:10.1073/pnas.0605064103.

Antonov, J. I., D. Seidov, T. P. Boyer, R. A. Locarnini, A. V. Mishonov, H. E. Garcia, O. K. Baranova, M. M. Zweng, and D. R. Johnson (2010), World Ocean Atlas 2009 Volume 2: Salinity, in *NOAA Atlas NESDIS 69*, edited by S. Levitus, p. 184, U.S. Gov. Printing Office, Washington, D.C.

Barnett, T. P., D. W. Pierce, and R. Schnur (2001), Detection of anthropogenic climate change in the world's oceans., *Science*, *292*(5515), 270–4, doi:10.1126/science.1058304.

Black, D. E., M. a. Abahazi, R. C. Thunell, A. Kaplan, E. J. Tappa, and L. C. Peterson (2007), An 8-century tropical Atlantic SST record from the Cariaco Basin: Baseline variability, twentieth-century warming, and Atlantic hurricane frequency, *Paleoceanography*, *22*(4), 1–10, doi:10.1029/2007PA001427.

Böhm, F., M. M. Joachimski, W.-C. Dullo, A. Eisenhauer, H. Lehnert, J. Reitner, and G. Wörheide (2000), Oxygen isotope fractionation in marine aragonite of coralline sponges, *Geochimica et Cosmochimica Acta*, *64*(10), 1695–1703, doi:10.1016/S0016-7037(99)00408-1.

Böhm, F., A. Haase-Schramm, A. Eisenhauer, W.-C. Dullo, M. M. Joachimski, H. Lehnert, and J. Reitner (2002), Evidence for preindustrial variations in the marine surface water carbonate system from coralline sponges, *Geochemistry Geophysics Geosystems*, *3*(3), doi:10.1029/2001GC000264.

Chen, A., and M. Taylor (2002), Investigating the link between early season Caribbean rainfall and the El Niño + 1 year, *International Journal of Climatology*, *22*(1), 87–106, doi:10.1002/joc.711.

Coplen, T. B. (1996), New guidelines for reporting stable hydrogen, carbon, and oxygen isotope-ratio data, *Geochimica et Cosmochimica Acta*, *60*(17), 3359–3360, doi:10.1016/0016-7037(96)00263-3.

Cullen, H. M., R. D. D'Arrigo, E. R. Cook, and M. E. Mann (2001), Multiproxy reconstructions of the North Atlantic Oscillation, *Paleoceanography*, *16*(1), 27, doi:10.1029/1999PA000434.

Delworth, T. L., and T. R. Knutson (2000), Simulation of Early 20th Century Global Warming, *Science*, *287*(5461), 2246–2250, doi:10.1126/science.287.5461.2246.

Dima, M., G. Lohmann, and I. Dima (2005), Solar-induced and internal climate variability at decadal time scales, *International Journal of Climatology*, *25*(6), 713–733, doi:10.1002/joc.1156.

Douglass, D. H., and B. D. Clader (2002), Climate sensitivity of the Earth to solar irradiance, *Geophysical Research Letters*, *29*(16), doi:10.1029/2002GL015345.

Enfield, D. B., and E. J. Alfaro (1999), The Dependence of Caribbean Rainfall on the Interaction of the Tropical Atlantic and Pacific Oceans, *Journal of Climate*, *12*(7), 2093–2103, doi:10.1175/1520-0442(1999)012<2093:TDOCRO>2.0.CO;2.

Enfield, D. B., A. M. Mestas-Nuñez, and P. J. Trimble (2001), The Atlantic Multidecadal Oscillation and its relation to rainfall and river flows in the continental U.S., *Geophysical Research Letters*, *28*(10), 2077, doi:10.1029/2000GL012745.

Fensterer, C. (2011), Holocene Caribbean climate variability reconstructed from speleothems from western Cuba, PhD Thesis., Ruperto-Carola University of Heidelberg, Heidelberg, Germany. [online] Available from: http://www.ub.uni-heidelberg.de/archiv/11621 (Accessed 1 August 2012)

Foster, L. C., C. Andersson, H. Høie, N. Allison, a. a. Finch, and T. Johansen (2008), Effects of micromilling on δ 18 O in biogenic aragonite, *Geochemistry Geophysics Geosystems*, *9*(4), 1–6, doi:10.1029/2007GC001911.

Giannini, A., Y. Kushnir, and M. A. Cane (2000), Interannual Variability of Caribbean Rainfall, ENSO, and the Atlantic Ocean*, *Journal of Climate*, *13*(2), 297–311, doi:10.1175/1520-0442(2000)013<0297:IVOCRE>2.0.CO;2.

Gill, I., J. J. Olson, and D. K. Hubbard (1995), Corals, paleotemperature records, and the aragonite-calcite transformation, *Geology*, *23*(4), 333, doi:10.1130/0091-7613(1995)023<0333:CPRATA>2.3.CO;2.

Gray, S. T. (2004), A tree-ring based reconstruction of the Atlantic Multidecadal Oscillation since 1567 A.D., *Geophysical Research Letters*, *31*(12), 2–5, doi:10.1029/2004GL019932.

Haase-Schramm, A., F. Böhm, A. Eisenhauer, W.-C. Dullo, M. M. Joachimski, B. Hansen, and J. Reitner (2003), Sr/Ca ratios and oxygen isotopes from sclerosponges: Temperature history of the Caribbean mixed layer and thermocline during the Little Ice Age, *Paleoceanography*, *18*(3), 1073, doi:10.1029/2002PA000830.

Hai, X. U., H. Yetang, and L. I. N. Qinghua (2002), Temperature variations in the past 6000 years inferred from δ 18 O of peat cellulose from Hongyuan , China, , *47*(18).

Hammer, Ø., D. A. T. Harper, and P. D. Ryan (2001), PAST: Paleontological Statistics Software Package for Education and Data Analysis, *Palaeontologia Electronica*, *4*(1). [online] Available from: http://palaeo-electronica.org/2001_1/past/issue1_01.htm

Hasselmann, K. (1976), Stochastic climate models Part I. Theory, *Tellus*, *28*(6), 473–485, doi:10.1111/j.2153-3490.1976.tb00696.x.

Haug, G. H., K. a Hughen, D. M. Sigman, L. C. Peterson, and U. Röhl (2001), Southward migration of the intertropical convergence zone through the Holocene., *Science*, *293*(5533), 1304–8, doi:10.1126/science.1059725.

Hickson, S. (1911), On Ceratopora, the type of a new family of Alcyonaria, *Proceedings of the Royal Society of London B*, *84*(570), 195–200.

Hong, Y. T., H. B. Jiang, T. S. Liu, X. G. Qin, L. P. Zhou, J. Beer, H. D. Li, and X. T. Leng (2000), Response of climate to solar forcing recorded in a 6000-year d 18 O time-series of Chinese peat cellulose, *The Holocene*, *10*(1), 1–7, doi:10.1191/095968300669856361.

Hughes, G. B., and C. W. Thayer (2001), Sclerosponges: potential high-resolution recorders of marine paleotemperatures, in *Geological perspectives of global climate change*, edited by L. Gerhard, W. Harrison, and B. Hanson, pp. 137–151, American Association Of Petroleum Geologists.

Huh, C.-A., and M. P. Bacon (1985), Thorium-232 in the eastern Caribbean Sea, *Nature*, *316*(6030), 718–721, doi:10.1038/316718a0.

Jiang, H., J. Eiríksson, M. Schulz, K.-L. Knudsen, and M.-S. Seidenkrantz (2005), Evidence for solar forcing of sea-surface temperature on the North Icelandic Shelf during the late Holocene, *Geology*, *33*(1), 73, doi:10.1130/G21130.1.

Jury, M., B. a. Malmgren, and A. Winter (2007), Subregional precipitation climate of the Caribbean and relationships with ENSO and NAO, *Journal of Geophysical Research*, *112*(D16), 1–10, doi:10.1029/2006JD007541.

Kara, a. B., P. a. Rochford, and H. E. Hurlburt (2000), An optimal definition for ocean mixed layer depth, *Journal of Geophysical Research*, *105*(C7), 16803, doi:10.1029/2000JC900072.

Kilbourne, K. H., T. M. Quinn, R. Webb, T. Guilderson, J. Nyberg, and A. Winter (2008), Paleoclimate proxy perspective on Caribbean climate since the year 1751: Evidence of cooler temperatures and multidecadal variability, *Paleoceanography*, *23*(3), 1–14, doi:10.1029/2008PA001598.

Knight, J. R., C. K. Folland, and A. a. Scaife (2006), Climate impacts of the Atlantic Multidecadal Oscillation, *Geophysical Research Letters*, *33*(17), 1–4, doi:10.1029/2006GL026242.

Latif, M. et al. (2004), Reconstructing, Monitoring, and Predicting Multidecadal-Scale Changes in the North Atlantic Thermohaline Circulation with Sea Surface Temperature, *Journal of Climate*, *17*(7), 1605–1614, doi:10.1175/1520-0442(2004)017<1605:RMAPMC>2.0.CO;2.

Lazareth, C., P. Willenz, J. Navez, and E. Keppens (2000), Sclerosponges as a new potential recorder of environmental changes: Lead in Ceratoporella nicholsoni, *Geology*, *28*(6), 515–518.

Lean, J. (2000), Evolution of the Sun's Spectral Irradiance Since the Maunder Minimum, *Geophysical Research Letters*, *27*(16), 2425, doi:10.1029/2000GL000043.

Lean, J. L., Y.-M. Wang, and N. R. Sheeley Jr. (2002), The effect of increasing solar activity on the Sun's total and open magnetic flux during multiple cycles: Implications for solar forcing of climate, *Geophysical Research Letters*, *29*(24), 2–5, doi:10.1029/2002GL015880.

Locarnini, R. A., A. V. Mishonov, J. I. Antonov, T. P. Boyer, H. E. Garcia, O. K. Baranova, M. M. Zweng, and D. R. Johnson (2010), World Ocean Atlas 2009 Volume 1: Temperature, in *NOAA Atlas NESDIS 68*, edited by S. Levitus, p. 184, U.S. Government Printing Office, Washington, D.C.

Malmgren, B. A., A. Winter, and D. Chen (1998), El Niño–Southern Oscillation and North Atlantic Oscillation Control of Climate in Puerto Rico, *Journal of Climate*, *11*(10), 2713–2717, doi:10.1175/1520-0442(1998)011<2713:ENOSOA>2.0.CO;2.

Meehl, G. a., W. M. Washington, T. M. L. Wigley, J. M. Arblaster, and A. Dai (2003), Solar and Greenhouse Gas Forcing and Climate Response in the Twentieth Century, *Journal of Climate*, *16*(3), 426–444, doi:10.1175/1520-0442(2003)016<0426:SAGGFA>2.0.CO;2.

Mickler, P. J., J. L. Banner, L. Stern, Y. Asmerom, R. L. Edwards, and E. Ito (2004), Stable isotope variations in modern tropical speleothems: Evaluating equilibrium vs. kinetic isotope effects, *Geochimica et Cosmochimica Acta*, *68*(21), 4381–4393, doi:10.1016/j.gca.2004.02.012.

Minobe, S., A. Kuwano-Yoshida, N. Komori, S. Xie, and R. J. Small (2008), Influence of the Gulf Stream on the troposphere., *Nature*, *452*(7184), 206–9, doi:10.1038/nature06690.

Nyberg, J., B. A. Malmgren, A. Kuijpers, and A. Winter (2002), A centennial-scale variability of tropical North Atlantic surface hydrography during the late Holocene, *Palaeogeography, Palaeoclimatology, Palaeoecology*, *183*(1-2), 25–41, doi:10.1016/S0031-0182(01)00446-1.

Regenberg, M., S. Steph, D. Nürnberg, R. Tiedemann, and D. Garbe-Schönberg (2009), Calibrating Mg/Ca ratios of multiple planktonic foraminiferal species with $\delta^{18}O$-calcification temperatures: Paleothermometry for the upper water column, *Earth and Planetary Science Letters*, *278*(3-4), 324–336, doi:10.1016/j.epsl.2008.12.019.

Reynaud-Vaganay, S., A. Juillet-Leclerc, J. Jaubert, and J.-P. Gattuso (2001), Effect of light on skeletal $\delta^{13}C$ and $\delta^{18}O$, and interaction with photosynthesis, respiration and calcification in two zooxanthellate scleractinian corals, *Palaeogeography, Palaeoclimatology, Palaeoecology*, *175*(1-4), 393–404, doi:10.1016/S0031-0182(01)00382-0.

Richardson, P. L. (2005), Caribbean Current and eddies as observed by surface drifters, *Deep Sea Research Part II: Topical Studies in Oceanography*, *52*(3-4), 429–463, doi:10.1016/j.dsr2.2004.11.001.

Richey, J. N., R. Z. Poore, B. P. Flower, and T. M. Quinn (2007), 1400 yr multiproxy record of climate variability from the northern Gulf of Mexico, *Geology*, *35*(5), 423, doi:10.1130/G23507A.1.

Rosenheim, B. E., P. K. Swart, S. R. Thorrold, P. Willenz, L. Berry, and C. Latkoczy (2004), High-resolution Sr/Ca records in sclerosponges calibrated to temperature in situ, *Geology*, *32*(2), 145–148, doi:10.1130/G20117.1.

Rosenheim, B. E., P. K. Swart, and S. R. Thorrold (2005), Minor and trace elements in sclerosponge Ceratoporella nicholsoni: Biogenic aragonite near the inorganic endmember?, *Palaeogeography, Palaeoclimatology, Palaeoecology*, *228*(1-2), 109–129, doi:10.1016/j.palaeo.2005.03.055.

Schimdt, G. A., G. R. Bigg, and E. J. Rohling (1999), Global Seawater Oxygen-18 Database - v1.21, [online] Available from: http://data.giss.nasa.gov/o18data/

Scholz, D., and D. Hoffmann (2008), 230Th/U-dating of fossil corals and speleothems, *Quaternary Science Journal*, *57*(1-2), 52–76, doi:10.3285/eg.57.1-2.3.

Scholz, D., A. Mangini, and T. Felis (2004), U-series dating of diagenetically altered fossil reef corals, *Earth and Planetary Science Letters*, *218*(1-2), 163–178, doi:10.1016/S0012-821X(03)00647-2.

Sherman, C., R. Appeldoorn, M. Carlo, M. Nemeth, H. Ruíz, and I. Bejarano (2009), Use of Technical Diving to Study Deep Reef Environments in Puerto Rico, in *Diving For Science 2009 Proceeding of the American Academy of Underwater Sciences 28th Scientific Symposium*, edited by N. W. Pollock, pp. 58–65, AAUS, Dauphin Island.

Shindell, D. T., G. a Schmidt, M. E. Mann, D. Rind, and A. Waple (2001), Solar forcing of regional climate change during the Maunder Minimum., *Science*, *294*(5549), 2149–52, doi:10.1126/science.1064363.

Smith, S. W. (1997), Moving average filters, in *The Scientist and Engineer's Guide to Digital Signal Processing*, pp. 277–284, California Technical Pub.

Smith, T. M., R. W. Reynolds, T. C. Peterson, and J. Lawrimore (2008), Improvements to NOAA's Historical Merged Land–Ocean Surface Temperature Analysis (1880–2006), *Journal of Climate*, *21*(10), 2283–2296, doi:10.1175/2007JCLI2100.1.

Stichler, W. (1995), Interlaboratory comparison of new materials for carbon and oxygen isotope ratio measurements, in *Reference and Intercomparison Materials for Stable Isotopes of Light Elements*, pp. 67–74, IAEA, Vienna.

Swart, P., J. Rubenstone, and C. Charles (1998), Sclerosponges: A new proxy indicator of climate, *NOAA Climate and Global Change Program Special Report*, (12).

Swart, P. K., S. Thorrold, B. Rosenheim, A. Eisenhauer, and C. G. A. Harrison (2002), Intra-annual variation in the stable oxygen and carbon and trace element composition of sclerosponges, *Paleoceanography*, *17*(3), 1045, doi:10.1029/2000PA000622.

Swart, P. K., L. Greer, B. E. Rosenheim, C. S. Moses, A. J. Waite, A. Winter, R. E. Dodge, and K. Helmle (2010), The ^{13}C Suess effect in scleractinian corals mirror changes in the anthropogenic CO_2 inventory of the surface oceans, *Geophysical Research Letters*, *37*(5), 1–5, doi:10.1029/2009GL041397.

Tett, S. F. B., P. A. Stott, M. R. Allen, W. J. Ingram, and J. F. B. Mitchell (1999), Causes of twentieth-century temperature change near the Earth's surface, *Nature*, (399), 569–572, doi:10.1038/21164.

Torrence, C., and G. P. Compo (1998), A Practical Guide to Wavelet Analysis, *Bulletin of the American Meteorological Society*, *79*(1), 61–78, doi:10.1175/1520-0477(1998)079<0061:APGTWA>2.0.CO;2.

Vieira, L. E. a., S. K. Solanki, N. a. Krivova, and I. Usoskin (2011), Evolution of the solar irradiance during the Holocene, *Astronomy & Astrophysics*, *531*, A6, doi:10.1051/0004-6361/201015843.

Wang, C., and D. B. Enfield (2001), The Tropical Western Hemisphere Warm Pool, *Geophysical Research Letters*, *28*(8), 1635, doi:10.1029/2000GL011763.

Waple, A. M., M. E. Mann, and R. S. Bradley (2002), Long-term patterns of solar irradiance forcing in model experiments and proxy based surface temperature reconstructions, , 563–578, doi:10.1007/s00382-001-0199-3.

White, W. B., J. Lean, D. R. Cayan, and M. D. Dettinger (1997), Response of global upper ocean temperature to changing solar irradiance, *Journal of Geophysical Research*, *102*(C2), 3255–3266, doi:10.1029/96JC03549.

Willenz, P., and W. D. Hartman (1989), Micromorphology and ultrastructure of Caribbean sclerosponges, *Marine Biology*, *103*(3), 387–401, doi:10.1007/BF00397274.

Winter, A., T. Miller, Y. Kushnir, A. Sinha, A. Timmermann, M. R. Jury, C. Gallup, H. Cheng, and R. L. Edwards (2011), Evidence for 800years of North Atlantic multi-decadal variability from a Puerto Rican speleothem, *Earth and Planetary Science Letters*, *308*(1-2), 23–28, doi:10.1016/j.epsl.2011.05.028.